Photonic structures of metal-coated chiral spheres

Aristi Christofi[1,2,*] and Nikolaos Stefanou[1]

[1]*University of Athens, Section of Solid State Physics, Panepistimioupolis, GR-157 84 Athens, Greece*
[2]*Institute of Materials Science, NCSR "Demokritos," GR-153 10 Athens, Greece*
**Corresponding author: aristi@ims.demokritos.gr*

Received December 21, 2011; revised February 20, 2012; accepted March 1, 2012;
posted March 6, 2012 (Doc. ID 160381); published May 9, 2012

A detailed analysis of the optical properties of photonic structures of metal-coated chiral spheres, calculated by the full electrodynamic layer-multiple-scattering method, is presented. Easily tunable narrow bands, originating from particle-like plasmon modes of the metallic shells, hybridize with the extended bands of the underlying effective chiral medium and give rise to sizable partial gaps and strong band bending with consequent negative-slope dispersion. The photonic band diagram is discussed in the light of group theory, in conjunction with relevant transmission spectra, and the occurrence of polarization-selective transmission and negative refraction for a short range of angles of incidence is demonstrated.

OCIS codes: 160.1585, 160.5298, 160.3918, 250.5403.

1. INTRODUCTION

Composite structures with chiral components are promising candidates for exotic optical functions as in photonic band engineering [1–4], nonlinear optics [5], and negative refraction [6–14]. On the other hand, the introduction of photonic resonances, such as localized plasmon modes, opens up impressive possibilities for tailoring the light-matter interaction and allows one to observe new, interesting, and potentially useful physical phenomena. In particular, it has been suggested that the existence of a chiral resonance, realized either in a mixture of small helical inclusions [8,10] or in an assembly of resonant particles in a nondispersive chiral medium [9], may lead to negative refraction and superlensing for one polarization.

In this paper, we seek to combine chirality and resonance on a single versatile building unit: a metal-coated chiral sphere. Chirality is provided by the core, while the metallic shell introduces plasmonic resonances. Plasmons of the outer and inner surfaces of the shell interact with each other and give rise to two predominant dipole hybrid modes, one below the lower (particle-like) and one above the higher (cavity-like) resonances, which can be easily tuned by properly adjusting the thickness of the shell [15–17]. By assembling such metal-coated chiral spheres into a periodic structure, one can realize a resonant chiral medium that shows a remarkable optical response, including polarization-selective transmission, splitting of circular-polarization modes with consequent negative-slope dispersion, and negative refraction within a tunable frequency range. These general features are not encountered in crystals of nonchiral metal-coated spheres [17]. On the other hand, homogeneous chiral spheres exhibit resonances only in the strong chirality regime [4] and do not offer a versatile platform for tailoring an effective resonant chiral medium.

The remaining of the paper is organized as follows. In Section 2, we develop a formalism to describe electromagnetic (EM) scattering by a single metal-coated chiral sphere and discuss the different resonant modes of such a composite particle. In Section 3, we undertake a comprehensive analysis of photonic dispersion diagrams and corresponding transmission spectra of a face-centered cubic (fcc) crystal of metal-coated chiral spheres, calculated by the full electrodynamic layer-multiple-scattering method. Moreover, we examine the occurrence of negative refraction at certain frequency regions and angles of incidence on a specific crystallographic surface of the crystal, by reference to relevant isofrequency contours obtained from detailed photonic band-structure calculations. Our results are summarized in Section 4.

2. RESONANT MODES OF A METAL-COATED CHIRAL SPHERE

We assume a spherical core-shell particle of total radius S, embedded in a homogeneous and isotropic medium (air in our case). The shell, of inner radius S_c and thickness D ($S = S_c + D$), is made of a metallic material with relative permeability $\mu_m = 1$ and dielectric function described by the simple, yet effective, Drude model [18]

$$\epsilon_m(\omega) = 1 - \frac{\omega_p^2}{\omega(\omega + i\tau^{-1})}, \tag{1}$$

where τ is the relaxation time of the conduction band electrons and ω_p is the bulk plasma frequency that naturally introduces c/ω_p as the length unit, $c = 1/\sqrt{\epsilon_0\mu_0}$ being the velocity of light in vacuum. We note that, assuming $\hbar\omega_p \simeq 10$ eV, c/ω_p corresponds to about 20 nm.

The core is made of a chiral material, which is described by the phenomenological Drude–Born–Fedorov constitutive relations [19]

$$\mathbf{D}(\mathbf{r}, t) = \epsilon_c\epsilon_0[\mathbf{E}(\mathbf{r}, t) + \beta_c\nabla \times \mathbf{E}(\mathbf{r}, t)], \tag{2}$$

$$\mathbf{B}(\mathbf{r}, t) = \mu_c\mu_0[\mathbf{H}(\mathbf{r}, t) + \beta_c\nabla \times \mathbf{H}(\mathbf{r}, t)], \tag{3}$$

where ϵ_c, μ_c denote the isotropic relative permittivity and permeability, respectively, and β_c is the chirality parameter, in

units of length, which can be deduced from experimental data for the specific rotatory power. Homogeneous plane waves propagating in this material have the form of circularly polarized waves of either handedness with wave numbers $q_L = q_c/(1 - q_c\beta_c)$ and $q_R = q_c/(1 + q_c\beta_c)$, for left- and right-circular polarization (LCP and RCP, respectively), where $q_c = \omega\sqrt{\epsilon_c\mu_c}/c$. We note that $\beta_c = c/\omega_p$ corresponds to a specific rotatory power of the order of $\sim 10^2$ degrees per sample thickness equal to one wavelength, at optical frequencies, which is much larger than that of naturally occurring optically active materials (a specific rotatory power as large as $7.2^\circ/\mu$m has been reported for poly-L-lactic acid in the visible range [20]). However, properly designed chiral metamaterials can exhibit a huge optical activity, which exceeds by several orders of magnitude that of naturally occurring optically active materials [11–13]. It is also worth noting that, assuming a constant value for β_c, the strength of chirality that can be quantified by the dimensionless parameter $q_c\beta_c$ vanishes in the static limit and increases linearly with frequency. Such an increase, and even stronger than linear, is encountered in optically active materials [21].

The core-shell particle under consideration is illuminated by a plane EM wave. The electric field associated with a time-harmonic, monochromatic EM wave, of angular frequency ω, has the form $\mathbf{E}(\mathbf{r}, t) = \mathrm{Re}[\mathbf{E}(\mathbf{r})\exp(-i\omega t)]$. In a homogeneous and isotropic medium, such as the metallic shell and the host, $\mathbf{E}(\mathbf{r})$ can be expanded, in general, into regular and irregular vector spherical waves of electric and magnetic type [22,23]. In the chiral core, since the wavefield must be finite at the origin, $\mathbf{E}(\mathbf{r})$ is expanded only into regular LCP and RCP vector spherical waves.

In the shell region, the expansion coefficients of the irregular vector spherical waves are related linearly with those of the regular vector spherical waves through the scattering matrix $\mathbf{T}$ that describes the chiral spherical core, embedded in the shell medium that extends (one assumes) to infinity [24]. We denote the matrix elements of $\mathbf{T}$ in the spherical-wave basis by $T_{Plm;P'l'm'}$, where P stands for the polarization mode, electric (E) or magnetic (H), and l, m are the usual angular momentum indices. Because of the spherical symmetry of the scatterer, $\mathbf{T}$ is diagonal in l and independent of m; however, it is not diagonal in P in the given representation, which reflects the mixing of the E and H modes because of chirality. Therefore $T_{Plm;P'l'm'} = T_{PP';l}\delta_{ll'}\delta_{mm'}$, with $T_{PP';l}$ given by [4,25]

$$T_{EE;l} = \frac{U_{L;l}C_{R;l} + U_{R;l}C_{L;l}}{U_{L;l}V_{R;l} + U_{R;l}V_{L;l}}, \tag{4}$$

$$T_{HH;l} = \frac{V_{L;l}D_{R;l} + V_{R;l}D_{L;l}}{U_{L;l}V_{R;l} + U_{R;l}V_{L;l}}, \tag{5}$$

$$T_{EH;l} = i\frac{U_{L;l}D_{R;l} - U_{R;l}D_{L;l}}{U_{L;l}V_{R;l} + U_{R;l}V_{L;l}} = -T_{HE;l}, \tag{6}$$

where

$$U_{L(R);l} = \sqrt{\frac{\epsilon_c\mu_m}{\epsilon_m\mu_c}}h_l^+(q_mS)\frac{1}{z}\frac{\partial[zj_l(z)]}{\partial z}\bigg|_{z=q_{L(R)}S} - j_l(q_{L(R)}S)\frac{1}{z}\frac{\partial[zh_l^+(z)]}{\partial z}\bigg|_{z=q_mS}, \tag{7}$$

$$V_{L(R);l} = h_l^+(q_mS)\frac{1}{z}\frac{\partial[zj_l(z)]}{\partial z}\bigg|_{z=q_{L(R)}S} - \sqrt{\frac{\epsilon_c\mu_m}{\epsilon_m\mu_c}}j_l(q_{L(R)}S)\frac{1}{z}\frac{\partial[zh_l^+(z)]}{\partial z}\bigg|_{z=q_mS}, \tag{8}$$

$$C_{L(R);l} = \sqrt{\frac{\epsilon_c\mu_m}{\epsilon_m\mu_c}}j_l(q_{L(R)}S)\frac{1}{z}\frac{\partial[zj_l(z)]}{\partial z}\bigg|_{z=q_mS} - j_l(q_mS)\frac{1}{z}\frac{\partial[zj_l(z)]}{\partial z}\bigg|_{z=q_{L(R)}S}, \tag{9}$$

$$D_{L(R);l} = j_l(q_{L(R)}S)\frac{1}{z}\frac{\partial[zj_l(z)]}{\partial z}\bigg|_{z=q_mS} - \sqrt{\frac{\epsilon_c\mu_m}{\epsilon_m\mu_c}}j_l(q_mS)\frac{1}{z}\frac{\partial[zj_l(z)]}{\partial z}\bigg|_{z=q_{L(R)}S}. \tag{10}$$

In the above equations, $q_m = \omega\sqrt{\epsilon_m\mu_m}/c$, and j_l and h_l^+ are spherical Bessel and Hankel functions, respectively.

Similarly, the expansion coefficients of the regular vector spherical waves in the shell can be linearly expressed in terms of their counterparts in the host region through appropriate expansion coefficients $C_{PP';l}$, $P, P' = E, H$. After some straightforward algebra, the boundary conditions of continuity of the tangential components of the EM field at the inner and outer surfaces of the shell lead to two 4×4 linear systems, for each value of $l = 1, 2, \ldots\ldots$ The solution of these systems gives both $C_{PP';l}$ and $T^{\mathrm{tot}}_{PP';l}$, the latter being the elements of the T matrix of the composite core-shell particle that relate the expansion coefficients of the scattered field (irregular vector spherical waves) with those of the incident field (regular vector spherical waves). The linear systems can be cast in the form

$$\begin{pmatrix} d_{11} & d_{12} & d_{13} & 0 \\ d_{21} & d_{22} & 0 & d_{24} \\ d_{31} & d_{32} & 0 & d_{34} \\ d_{41} & d_{42} & d_{43} & 0 \end{pmatrix}\begin{pmatrix} C_{HH;l} & C_{HE;l} \\ C_{EH;l} & C_{EE;l} \\ T^{\mathrm{tot}}_{HH;l} & T^{\mathrm{tot}}_{HE;l} \\ T^{\mathrm{tot}}_{EH;l} & T^{\mathrm{tot}}_{EE;l} \end{pmatrix} = \begin{pmatrix} a_1 & 0 \\ 0 & -a_2 \\ 0 & a_1 \\ a_2 & 0 \end{pmatrix}, \tag{11}$$

where $d_{11} = j_l(q_mS) + T_{HH;l}h_l^+(q_mS)$, $d_{12} = T_{HE;l}h_l^+(q_mS)$, $d_{13} = -h_l^+(qS)$, $d_{21} = iT_{EH;l}[h_l^+(q_mS)/(q_mS) + h_l^{+\prime}(q_mS)]$, $d_{22} = i\{j_l(q_mS)/(q_mS) + j_l'(q_mS) + T_{EE;l}[h_l^+(q_mS)/(q_mS) + h_l^{+\prime}(q_mS)]\}$, $d_{24} = -i[h_l^+(qS)/(qS) + h_l^{+\prime}(qS)]$, $d_{31} = \sqrt{\epsilon_m\mu/\epsilon\mu_m}T_{EH;l}h_l^+(q_mS)$, $d_{32} = \sqrt{\epsilon_m\mu/\epsilon\mu_m}[T_{EE;l}h_l^+(q_mS) + j_l(q_mS)]$, $d_{34} = -h_l^+(qS)$, $d_{41} = -i\{j_l(q_mS)/(q_mS) + j_l'(q_mS) + T_{HH;l}[h_l^+(q_mS)/(q_mS) + h_l^{+\prime}(q_mS)]\}$, $d_{42} = -iT_{HE;l}[h_l^+(q_mS)/(q_mS) + h_l^{+\prime}(q_mS)]$, $d_{43} = i[h_l^+(qS)/(qS) + h_l^{+\prime}(qS)]$, and $a_1 = j_l(qS)$, $a_2 = -i[j_l(qS)/(qS) + j_l'(qS)]$, with $q = \omega/c$.

The scattering cross section associated with the incident plane-wave, normalized to the geometric cross section, can be expressed in terms of the scattering T matrix of the composite particle as follows [26]:

$$\sigma_{sc} = \frac{2}{(qS)^2}\sum_{l=1}^{\infty}(2l+1)[|T^{tot}_{EE;l}|^2 + |T^{tot}_{HH;l}|^2 + 2|T^{tot}_{EH;l}|^2]. \quad (12)$$

Let us consider a core-shell sphere of radius $S = 3.3c/\omega_p$ embedded in air. The shell, of inner radius $S_c = 3c/\omega_p$ and thickness $D = 0.3c/\omega_p$, is described by the Drude dielectric function of Eq. (1) without dissipative losses ($\tau^{-1} = 0$) and $\mu_m = 1$. The core is made of a chiral material with $\beta_c = 1.5c/\omega_p$, $\epsilon_c = 2$, and $\mu_c = 1$. The chiral core of the composite particle supports resonant modes of the EM field at high frequencies where chirality becomes strong enough [4]. On the other hand, the metallic shell supports particle plasmon modes, where the EM field is localized mostly at the outer surface of the shell, and cavity plasmon modes, where the EM field is localized mostly at the inner surface of the shell. Both modes are of electric 2^l-pole type and have been analyzed in detail elsewhere [15–17]. Plasmons of the outer and inner surfaces of the shell interact with each other and give rise to coupled modes, one below the lower (particle-like) and one above the higher (cavity-like) modes, which can be easily tuned by properly adjusting the thickness of the shell [15–17]. In the scattering cross section displayed in Fig. 1, the resonant modes of the chiral core and the particle-like plasmonic modes of the metallic shell are clearly visible. The cavity-like plasmonic modes appear at higher frequencies ($>0.8\omega_p$), and are not in the frequency region of interest. If we set $\beta_c = 0$, the chiral resonances disappear, thus allowing us to distinguish and identify the origin of the various modes. The fundamental dipole particle-like plasmon mode appears at $0.18\omega_p$, the quadrupole at $0.24\omega_p$, the octapole at $0.28\omega_p$, etc. Correspondingly, the fundamental dipole resonant mode of the chiral core appears at $0.31\omega_p$ and the quadrupole at $0.34\omega_p$.

3. PHOTONIC CRYSTALS OF METAL-COATED CHIRAL SPHERES

A. Description of the Crystal and Method of Calculation

We shall investigate in detail a particular example of an fcc crystal of the metal-coated chiral spheres considered in the previous section, with lattice constant $a = 10c/\omega_p$. We view the crystal as a sequence of (001) crystallographic planes. In each plane, the spheres are arranged on a square lattice, of lattice constant $a_0 = a\sqrt{2}/2$, while consecutive planes are separated by a distance $d = a/2$. Since the given crystal lacks invariance under space inversion because of the chiral material, the appropriate point symmetry group is O, which consists of only proper rotations, and not O_h that would be if the cores of the spheres were optically inactive [27].

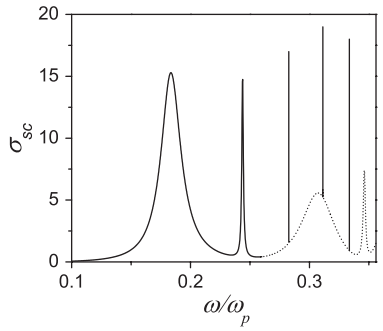

Fig. 1. The scattering cross section of a spherical particle consisting of a chiral core ($\beta_c = 1.5c/\omega_p$, $\epsilon_c = 2$, $\mu_c = 1$) of radius $S_c = 3c/\omega_p$, coated by a metallic shell, of thickness $D = 0.3c/\omega_p$, described by the Drude dielectric function without dissipative losses and $\mu_m = 1$. The particle is embedded in air. Solid and dotted lines denote particle-like plasmon and chiral resonances, respectively.

We calculate the photonic eigenmodes and the optical response of this crystal by the full electrodynamic layer-multiple-scattering method [22,23], which is ideally suited for the case under consideration. Besides the complex photonic band structure of the infinite crystal, the method allows one to calculate, also, the reflectance of the semi-infinite crystal as well as the reflectance and transmittance of a finite slab of the crystal, at any angle of incidence and, in this respect, it can describe an actual transmission experiment. Another advantage of the method is that it solves Maxwell equations in frequency domain and, therefore, it can treat dispersive materials, such as chiral substances and metals, and include dissipative losses in a straightforward manner. The properties of the individual scatterers enter only through the corresponding T matrix. At a first step, in-plane multiple scattering is evaluated in the spherical-wave basis using proper propagator functions. Subsequently, interlayer scattering is calculated in a plane-wave basis through appropriate transmission and reflection matrices, by including all propagating and evanescent components of the wave field necessary to obtain convergence. Therefore, interaction between the scatterers is fully taken into account. Explicit expressions for the propagator functions and the transmission and reflection matrices can be found elsewhere [22,23]. The scattering S matrix of a multilayer slab, which transforms the incident into the outgoing wave field, is obtained by combining the transmission and reflection matrices of the component layers. The ratio of the transmitted or reflected energy flux to the energy flux associated with the incident wave defines the transmittance or reflectance of the slab, respectively. On the other hand, for a three-dimensional crystal consisting of an infinite periodic sequence of layers, stacked along the z direction, applying Bloch theorem for the wave field in the region between two consecutive unit slabs leads to an eigenvalue equation, which gives the z component of the Bloch wave vector, k_z, for the given angular frequency ω and in-plane-wave vector component reduced within the surface Brillouin zone, $\mathbf{k}_\parallel$, which are conserved quantities in the scattering process. The eigenvalues $k_z(\omega, \mathbf{k}_\parallel)$, looked upon as functions of real ω, define, for each $\mathbf{k}_\parallel$, lines in the complex k_z plane. Taken together, they constitute the complex band structure of the infinite crystal associated with the given crystallographic plane. A line of given $\mathbf{k}_\parallel$ may be real (in the sense that k_z is real) over certain frequency regions, and be complex (in the sense that k_z is complex) for ω outside these regions. It turns out that, for given $\mathbf{k}_\parallel$ and ω, out of the eigenvalues $k_z(\omega, \mathbf{k}_\parallel)$, none or, at best, a few are real and the corresponding eigenvectors represent propagating modes of the EM field in the given infinite crystal. The remaining eigenvalues $k_z(\omega, \mathbf{k}_\parallel)$ are complex, and the corresponding eigenvectors represent evanescent waves. These have an amplitude that increases exponentially in the positive or negative z direction and, unlike the propagating waves, do not exist as

physical entities in the infinite crystal. However, they are an essential part of the physical solutions of the EM field in a slab of finite thickness. A region of frequency where propagating waves do not exist, for given $\mathbf{k}_{\|}$, constitutes a frequency gap of the EM field for the given $\mathbf{k}_{\|}$. If over a frequency region no propagating wave exists whatever the value of $\mathbf{k}_{\|}$, then this region constitutes an absolute frequency gap. In order to ensure adequate convergence in our calculations for the structure under consideration, it is sufficient to truncate the spherical-wave expansions at $l_{\max} = 5$ and take into account 37 two-dimensional reciprocal lattice vectors in the relevant plane-wave expansions [22,23].

B. Photonic Band Structure and Light Transmission

In Fig. 2, we display the calculated photonic band structure of the given crystal along its [001] direction. The bands along this direction can be classified according to the irreducible representations (A, B, E_1, E_2) of the C_4 group, which is a subgroup of O [27]. All these bands are nondegenerate, since the irreducible representations of C_4 are one dimensional. The E_1 and E_2 bands have the symmetry of LCP and RCP propagating waves, respectively, and thus can be excited by a wave of the appropriate polarization, incident normally on the (001) surface of the crystal. The A and B bands cannot be excited by an externally incident wave because they do not have the proper symmetry. In a finite (001) slab of the crystal, these bands correspond to bound states of the EM field that decrease exponentially outside the slab on either side of it.

The eigenmodes at the center of the Brillouin zone, $\mathbf{k} = (0, 0, 0)$, have the symmetry of the full O point group, while at the boundaries of the Brillouin zone, $\mathbf{k} = (0, 0, \pm\pi/d)$, they have the symmetry of the D_4 point group, which is also a subgroup of O. Group theory dictates that the optically active LCP and RCP bands along the [001] direction, of E_1 and E_2 symmetry, respectively, converge to doubly degenerate modes at the corresponding boundaries of the Brillouin zone and to threefold degenerate modes at the center of the Brillouin zone [4]. We note that polarization decomposition and existence of optically inactive bands apply only along high-symmetry directions, such as [001] or [111]. Along an arbitrary direction, all bands belong to the identity representation of the trivial group and thus can be excited by an appropriately incident wave of any polarization.

In Fig. 2, at low frequencies (below $\omega/\omega_p \approx 0.17$), we identify two nondegenerate extended bands of LCP and RCP

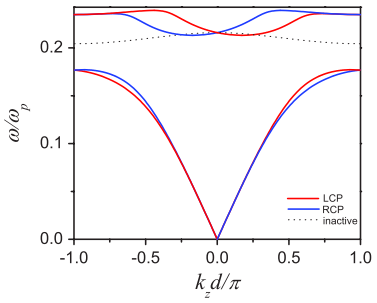

Fig. 2. (Color online) The photonic band structure of an fcc crystal, with lattice constant $a = 10c/\omega_p$, of chiral spheres ($\beta_c = 1.5c/\omega_p$, $\epsilon_c = 2$, $\mu_c = 1$) of radius $S_c = 3c/\omega_p$, coated with a metallic shell, of thickness $D = 0.3c/\omega_p$, described by the Drude dielectric function without dissipative losses and $\mu_m = 1$, along the [001] direction.

modes, of E_1 and E_2 symmetry, respectively, as expected for propagation in a homogeneous effective chiral medium, in the reduced-zone representation because of structure periodicity. In the frequency region about $\omega \approx 0.2\omega_p$, the photonic band structure is characterized by the presence of three additional narrow bands, one of E_1, one of E_2, and one of A symmetry, which originate from the dipole particle-like plasmon modes of the individual metal-coated chiral spheres, weakly interacting between them. The E_1 and E_2 narrow bands interact with the extended effective-medium bands of the same symmetry to produce the band diagram shown in Fig. 2. It can be seen that anticrossing interactions lead to strong band bending and negative-slope dispersion inside the Brillouin zone, along with a frequency gap extending from $0.179\omega_p$ to $0.211\omega_p$ in the given direction.

As mentioned above, along an arbitrary direction of the Brillouin zone, all bands belong to the identity representation of the trivial group and thus can be excited by an appropriately incident wave of any polarization. Moreover, in this case, anticrossing interaction between bands always takes place and removes degeneracies to a major or minor degree depending on the shape of the modes involved. In Fig. 3, we display the photonic band structure of the given crystal, along an arbitrary direction that corresponds to $\mathbf{k}_{\|} = (0.15, 0)2\pi/a_0$. In this case, the bands cannot be classified as of purely LCP or RCP character, but there is a different degree of LCP and RCP admixture that varies along a specific band as shown in Fig. 3. Characterizing the band eigenmodes in this way is consistent with corresponding transmission spectra of finite slab of the given crystal, for $\mathbf{k}_{\|} = (0.15, 0)2\pi/a_0$. Modes with a certain predominant circular-polarization character and positive (negative) group velocity couple predominantly to a plane EM wave with the same polarization, incident along the positive (negative) z direction on a (001) slab of the crystal. As shown in Fig. 4, over the frequency range of a polarization gap, only incident waves of opposite handedness are allowed to pass through. In the inset of Fig. 4, we depict the variation of the transmittance of a slab consisting of silver-coated chiral spheres, versus the angle of incidence, θ, for RCP incident light at a specific frequency where a corresponding gap opens up off the normal direction. It can be seen that for $\theta \geq 15°$, the RCP component of an incident light beam is filtered out.

C. Isofrequency Contours and Negative Refraction

We now investigate the possibility of negative refraction in the crystal under consideration, by examining the direction of the relevant group velocities obtained from the exact form of the calculated isofrequency surfaces. As can be seen in Fig. 2, chirality splits the LCP and RCP components of the degenerate transverse modes and in doing so creates a short range of frequencies just below the intersection point of the bands at the center of the Brillouin zone, about $0.21\omega_p$, where the group velocity has the opposite sign to the phase velocity ($k_z \partial\omega/\partial k_z < 0$) for a specific polarization, which is the signature of negative refraction. This mechanism for chiral negative refraction has also been demonstrated by others [9,14] and is a general one. Only the ingredients of a resonant system producing a band gap and chirality are needed. It is worth noting that the characteristic dimensions in the structure under study, i.e., particle size and interparticle distance, are 4–5

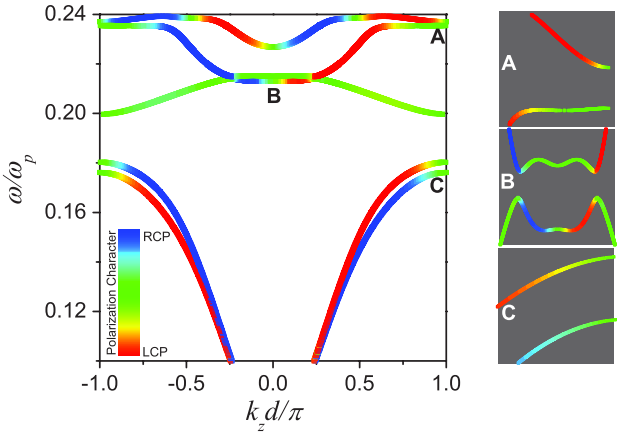

Fig. 3. (Color online) The photonic band structure of the crystal under consideration for $\mathbf{k}_{\parallel} = (0.15, 0)2\pi/a_0$. An enlarged view of the dispersion diagram in regions A, B, C is shown in the margin.

times smaller than the wavelength ($\lambda \sim 30c/\omega_p$). Figure 5 displays isofrequency contours, $\omega(\mathbf{k}) = \text{const.}$, in the $k_x - k_z$ plane ($k_y = 0$), in the frequency region of interest, which are appropriate for the description of the refractive properties of the crystal when the plane of incidence is the x–z plane. This corresponds to incidence on the x–y and on the y–z crystallographic surfaces, with $k_y = 0$.

If a plane EM wave of angular frequency ω impinges on the $x - y$ surface of the crystal with $\mathbf{q}_{\parallel} = \mathbf{k}_{\parallel} = (k_x, 0)$, the wavevector component parallel to the surface, k_x, is conserved and thus the points of the corresponding isofrequency curves with the same specific value of their k_x coordinate provide all possible wavevectors for the transmitted waves. The actual transmitted waves are determined from the proper direction of the corresponding group velocity, $\mathbf{v} = \nabla_{\mathbf{k}}\omega(\mathbf{k})$, which must be pointing inside the crystal because of causality. For example, if the crystal occupies the $z > 0$ half-space, v_z must be positive. A careful inspection of Fig. 6 reveals that, for light of angular frequency $\omega = 0.214\omega_p$ incident from air, we can have $k_x v_x < 0$, i.e., negative refraction. More specifically, we obtain a single negatively refracted beam for $0.04 < k_x a_0/\pi < 0.11$, which corresponds to angles of incidence ranging from ~5°

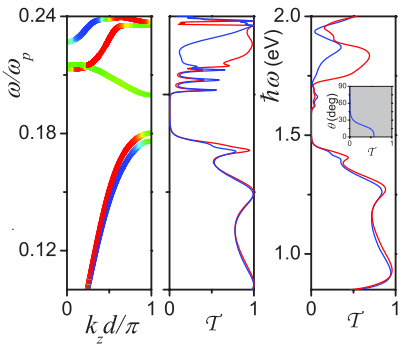

Fig. 4. (Color online) The photonic band structure of Fig. 3 for positive values of k_z (left-hand diagram) and the corresponding transmission spectra of a (001) slab of the crystal, four layers thick, for LCP (red line) and RCP (blue line) incident light (middle diagram). The right-hand diagram displays the corresponding transmission spectra if the metallic shell is described by the experimental dielectric function of bulk silver [28], which includes dissipative losses. The variation of the transmittance of this slab versus the angle of incidence, θ, for RCP incident light of frequency $\hbar\omega = 1.8$ eV is shown in the inset.

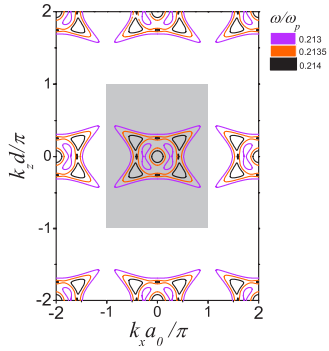

Fig. 5. (Color online) Isofrequency contours in the k_x–k_z plane ($k_y = 0$) for the crystal under consideration. The shaded rectangle shows the projection of the Brillouin zone on this plane.

to ~13°. Choosing a particular value of $k_x a_0/\pi = 0.05$, the k_x-conservation line crosses the relevant isofrequency contour of the crystal at two points, P and P'. The Bloch wave defined at point P' is backward propagating with respect to the interface and thus it is not a physically acceptable transmitted wave. Therefore, we obtain a single negatively refracted beam from point P, as shown in Fig. 6. For smaller angles of incidence, the k_x-conservation line also crosses the second branches of the isofrequency contour in the crystal (at larger values of k_z), and we may also have additional positively and negatively refracted beams. For larger angles of incidence, also positively and negatively refracted beams are simultaneously exited.

If we consider incidence on the y–z surface of the crystal with $\mathbf{q}_{\parallel} = \mathbf{k}_{\parallel} = (0, k_z)$, the conserved wavevector component parallel to the surface is k_z, and then we can also have $k_z v_z < 0$, i.e., negative refraction, as shown in Fig. 7 for light of angular frequency $\omega = 0.214\omega_p$ incident from air. In this case, we obtain a single negatively refracted beam for $0.037 < k_z d/\pi < 0.086$, which corresponds to a very short range of angles of incidence from ~3° to ~7°. Choosing $k_z d/\pi = 0.05$, the k_z-conservation line crosses the relevant isofrequency contour of the crystal at two points, P and P'. The Bloch wave defined at point P' is backward propagating

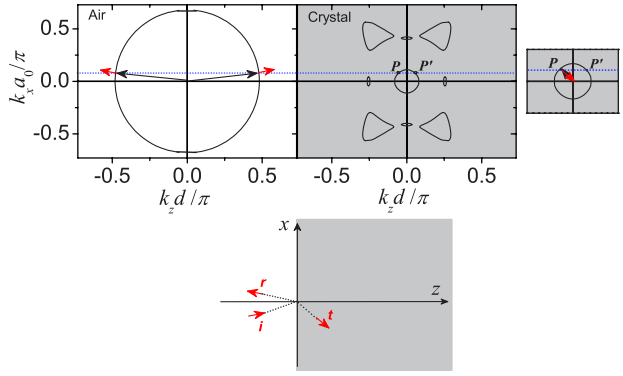

Fig. 6. (Color online) Isofrequency-contour analysis of the refraction of light of angular frequency $\omega = 0.214\omega_p$ incident from air on the x–y surface of the crystal under study with $k_y = 0$. The wavevectors and group velocities of the incident (i), reflected (r), and transmitted (t) waves are indicated by long and short arrows, respectively. An enlarged view of the transmitted wavevector and group velocity is displayed in the margin. The dotted horizontal line in the top diagrams is the k_x-conservation line. Negative refraction in real space is shown in the bottom diagram.

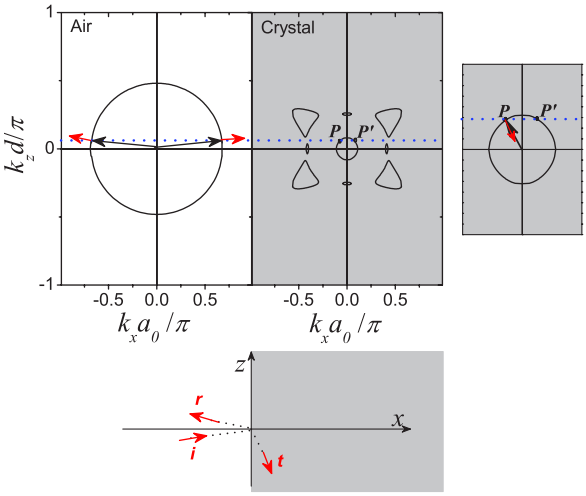

Fig. 7. (Color online) Isofrequency-contour analysis of the refraction of light of angular frequency $\omega = 0.214\omega_p$ incident from air on the $y-z$ surface of the crystal under study with $k_y = 0$. The wavevectors and group velocities of the incident (i), reflected (r), and transmitted (t) waves are indicated by long and short arrows, respectively. An enlarged view of the transmitted wavevector and group velocity is displayed in the margin. The dotted horizontal line in the top diagrams is the k_z-conservation line. Negative refraction in real space is shown in the bottom diagram.

with respect to the interface and thus it is not a physically acceptable transmitted wave. Therefore, we obtain a single negatively refracted beam from point P, as shown in Fig. 7. It is worth noting that, at smaller angles of incidence, the k_z-conservation line also crosses the second branches of the specific isofrequency contour in the crystal (at larger values of k_x) and a positively refracted beam is also excited. For larger angles of incidence, we always have regular refraction.

In view of the restricted range of angles of incidence for which a single negatively refracted beam is obtained, it should be stressed that negative refraction cannot be simply deduced from the existence of a band with negative slope and assignment of a scalar refractive index that refers to a specific mode and a particular direction of propagation. A direct demonstration that takes into account the full photonic band structure based, e.g., on the exact form of the isofrequency surfaces, is necessary.

4. CONCLUSIONS

In summary, we reported a thorough theoretical study of the optical properties of an fcc photonic crystal of metal-coated chiral spheres, by means of rigorous, full electrodynamic calculations using the layer-multiple-scattering method. We analyzed photonic band diagrams, in conjunction with relevant polarization-resolved transmission spectra for normal incidence or incidence at an angle on a given surface of the crystal, in the light of group theory. We explained the nature of the different eigenmodes of the EM field and revealed the existence of partial directional gaps, which can be easily tuned by a proper choice of the geometric parameters of the metal-coated chiral spheres and allow for polarization-selective transmission within a narrow range of angles of incidence. Finally, we investigated the possibility of negative refraction in the frequency region of a band with negative slope along the [001] direction. By carefully analyzing the corresponding isofrequency surfaces, we found that negative refraction takes place only for a short range of angles of incidence.

ACKNOWLEDGMENTS

A. Christofi was supported by the National Centre for Scientific Research "Demokritos" through a postgraduate fellowship.

REFERENCES

1. J. Chongjun, Q. Bai, Y. Miao, and Q. Ruhu, "Two-dimensional photonic band structure in the chiral medium transfer matrix method," Opt. Commun. **142**, 179–183 (1997).
2. I. E. Psarobas, N. Stefanou, and A. Modinos, "Photonic crystals of chiral spheres," J. Opt. Soc. Am. A **16**, 343–347 (1999).
3. C. He, M. H. Lu, R. C. Yin, T. Fan, and Y. F. Chen, "Chiral properties in a two-dimensional chiral polaritonic photonic crystal," J. Appl. Phys. **108**, 073103 (2010).
4. A. Christofi, N. Stefanou, and G. Gantzounis, "Photonic eigenmodes and light propagation in periodic structures of chiral nanoparticles," Phys. Rev. B **83**, 245126 (2011).
5. U. Gubler and C. Bosshard, "Optical material: a new twist for nonlinear optics," Nat. Mater. **1**, 209–210 (2002).
6. A. N. Lagarkov, V. N. Semenenko, V. A. Chistyaev, D. E. Ryabov, S. A. Tretyakov, and C. R. Simovski, "Resonance properties of Bi-Helix media at microwaves," Electromagnetics **17**, 213–237 (1997).
7. A. N. Lagarkov, V. N. Semenenko, V. N. Kisel, and V. A. Chistyaev, "Development and simulation of microwave artificial magnetic composites utilizing nonmagnetic inclusions," J. Magn. Magn. Mater. **258–259**, 161–166 (2003).
8. S. Tretyakov, I. Nefedov, A. Sihvola, S. Maslovski, and C. Simovski, "Waves and energy in chiral nihility," J. Electromagn. Waves. Appl. **17**, 695–706 (2003).
9. J. B. Pendry, "A chiral route to negative refraction," Science **306**, 1353–1355 (2004).
10. C. Monzon and D. W. Forester, "Negative refraction and focusing of circularly polarized waves in optically active media," Phys. Rev. Lett. **95**, 123904 (2005).
11. S. Zhang, Y. S. Park, J. Li, X. C. Lu, W. Zhang, and X. Zhang, "Negative refractive index in chiral metamaterials," Phys. Rev. Lett. **102**, 023901 (2009).
12. E. Plum, J. Zhou, J. Dong, V. A. Fedotov, T. Koschny, C. M. Soukoulis, and N. I. Zheludev, "Metamaterial with negative index due to chirality," Phys. Rev. B **79**, 035407 (2009).
13. X. Xiong, W. H. Sun, Y. J. Bao, M. Wang, R. W. Peng, C. Sun, X. Lu, J. Shao, Z. F. Li, and N. B. Ming, "Construction of a chiral metamaterial with a U-shaped resonator assembly," Phys. Rev. B **81**, 075119 (2010).
14. C. Wu, H. Li, Z. Wei, X. Yu, and C. T. Chan, Phys. Rev. Lett. **105**, 247401 (2010).
15. E. Prodan, C. Radloff, N. J. Halas, and P. Nordlander, "A hybridization model for the plasmon response of complex nanostructures," Science **302**, 419–422 (2003).
16. T. V. Teperik, V. V. Popov, and F. J. G. de Abajo, "Radiative decay of plasmons in a metallic nanoshell," Phys. Rev. B **69**, 155402 (2004).
17. C. Tserkezis, G. Gantzounis, and N. Stefanou, "Collective plasmonic modes in ordered assemblies of metallic nanoshells," J. Phys. Condens. Matter **20**, 075232 (2008).
18. N. W. Ashcroft and N. D. Mermin, *Solid State Physics* (Saunders, 1976).
19. A. Lakhtakia, *Beltrami Fields in Chiral Media* (World Scientific, 1994).
20. Y. Tajitsu, R. Hosoya, T. Maruyama, M. Aoki, Y. Shikinami, M. Date, and E. Fukada, "Huge optical rotatory power of uniaxially oriented film of poly-L-lactic acid," J. Mater. Sci. Lett. **18**, 1785–1787 (1999).
21. A. Yariv and P. Yeh, *Optical Waves in Crystals* (Wiley, 1984).
22. N. Stefanou, V. Yannopapas, and A. Modinos, "Heterostructures of photonic crystals: frequency bands and transmission coefficients," Comput. Phys. Commun. **113**, 49–77 (1998).
23. N. Stefanou, V. Yannopapas, and A. Modinos, "MULTEM2: a new version of the program for transmission and band-structure

calculations of photonic crystals," Comput. Phys. Commun. **132**, 189–196 (2000).
24. N. Stefanou, C. Tserkezis, and G. Gantzounis, "Plasmonic excitations in ordered assemblies of metallic nanoshells," Proc. SPIE **6989**, 698910 (2008).
25. C. F. Bohren, "Light scattering by an optically active sphere," Chem. Phys. Lett. **29**, 458–462 (1974).
26. C. F. Bohren and D. R. Huffman, *Absorption and Scattering of Light by Small Particles* (Wiley, 1983).
27. J. F. Cornwell, *Group Theory and Electronic Energy Bands in Solids* (North-Holland, 1969).
28. P. B. Johnson and R. W. Christy, "Optical constants of the noble metals," Phys. Rev. B **6**, 4370–4379 (1972).